International Soil and Water Conservation Research xxx (xxxx) xxx

Contents lists available at ScienceDirect

International Soil and Water Conservation Research

journal homepage: www.elsevier.com/locate/iswcr

Original Research Article

VIS-NIR spectroscopy and environmental factors coupled with PLSR models to predict soil organic carbon and nitrogen

Jingrong Zhu [a], Yihua Jin [a], Weihong Zhu [b, c, *], Dong Kun Lee [d]

[a] College of Agriculture, Yanbian University, Jilin, China
[b] College of Geography and Ocean Sciences, Yanbian University, Jilin, China
[c] Jilin Provincial Key Laboratory of Wetland Ecological Functions and Ecological Security, Hunchun, China
[d] Department of Landscape Architecture and Rural System Engineering, Seoul National University, Seoul, South Korea

ARTICLE INFO

Article history:
Received 30 May 2023
Received in revised form
31 January 2024
Accepted 2 February 2024
Available online xxx

Keywords:
DEM
NDVI
Spectra
PLSR
TWI

ABSTRACT

Soil profile organic carbon (OC) and total nitrogen (TN) are influenced by topographic attributes, and land use. The visible and near-infrared (Vis-NIR) spectroscopy method can be used for the prediction of OC and TN because it is reliable, nondestructive, fast, and cost-effective. VIS-NIR soil spectral and environmental data were combined with the Partial least squares regression (PLSR) model to examine the effect of topography attributes and land use on topsoil and subsoil OC and TN stocks. After this, based on the soil depth, 114 soil samples were collected from 0 to 20 cm (topsoil) and 20–50 cm (subsoil) under three land uses, as well as OC and TN, along with several soil properties including soil particles (sand, silt, clay), pH, and bulk density in both topsoil and subsoil samples were measured. A DEM with a resolution of 30 m was used to derive the topography factors and remote sensing data was used to calculate the vegetation index. Soils (0–50 cm) under orchard land use had the highest stock of SOC (7.4 kg m^{-2}) as well as TN (2.4 kg m^{-2}). There was a significant increase in the organic matter stock of soils located on the south aspect (8.3 kg m^{-2}) compared to soils located on other aspects, particularly on the north aspect (3.9% increase). Soils on the south aspect contain higher soil-water contents and lower temperatures, resulting in a decrease in the decomposition of soil organic matter. A strong positive correlation was demonstrated between topography wetness index (0.57–0.63) and topography TN stocks (0.54–0.66) as well as the highest loading score among terrain attributes, suggesting that topography is the primary factor controlling SOC stocks, particularly subsoil stocks. Additionally, we found that soils on the south-facing aspects (N aspects) had the highest spectra. Additionally, the PLSR, which showed an R^2 of 0.82, a RMSE of 0.15 %, and a RPD of 0.39 indicated excellent prediction capabilities for the OC content. We concluded that the PLSR model coupled with Vis-NIR spectroscopy is able to predict topsoil and subsoil OC and N content under different aspect slopes.

1. Introduction

The largest terrestrial storage of carbon (C) is situated in the soil. and is a major source of atmospheric CO2 (Alcántara et al., 2016). In addition to contributing to soil fertility and soil water retention, soil organic carbon (SOC) also helps prevent soil degradation and reduces atmospheric CO_2 emissions (Adhikari & Hartemink, 2016). Maintaining SOC stocks and their related functions requires an understanding of the mechanisms that affect their stability (Matteodo et al., 2018). Enhancing SOC storage has been advocated for decades, and recently, it has been argued that enhancing SOC by 4% per year in agricultural soils can offset global greenhouse gas emissions from agriculture (Osanai et al., 2020). A primary nutrient for plants, nitrogen is one of the macronutrients required in large amounts for metabolism and growth. Nitrogen storage in soil is affected by climate through biotic processes such as vegetation production and the decomposition of organic matter.

* Corresponding author. College of Geography and Ocean Sciences, Yanbian University, Jilin, China.
E-mail addresses: jr.zhu@ybu.edu.cn (J. Zhu), jinyh2018@ybu.edu.cn (Y. Jin), whzhu@ybu.edu.cn (W. Zhu), dklee7@snu.ac.kr (D.K. Lee).

https://doi.org/10.1016/j.iswcr.2024.02.001

The subsoil is the layer of soil below the topsoil, containing minerals and leached metals. The subsoil plays a crucial role in water drainage and root penetration. While the topsoil is the uppermost layer where most of the plant roots and organic material are concentrated, the subsoil provides structural support and can influence the availability of water and nutrients to plants. Contrary to topsoil, subsoil primarily consists of low SOC content and high radio C, which indicates high SOC stability gradually turned to using deeper soil and precipitation (Qiu et al., 2023). Globally, terrestrial carbon flux balances in global carbon cycle (Jia & Zhou, 2023), and it is estimated than half of the SOC is stored at the surface layer (Batjes, 2014). Therefore, subsoil C might be an even more important sink for CO_2 than topsoil, but it is, to date, poorly understood, and most of the studies on SOC have mainly focused on deep <30 cm with the highest SOC content. The main reasons for this globally ignorance of subsoil SOC consist of the time-consuming, costly, and laborious task of subsoil sampling and traditional beliefs that subsoil SOC is old, stable, and insensitive to environmental changes (Liu et al., 2020).

There is no doubt that topography plays a significant role in the function of soil, thus profoundly influencing the content of soil organic matter (SOM). (Ferretti, 2019). Various factors related to topography are responsible for the intensity and process of land degradation and soil sedimentation, organic fractions, and nutrient availability (Schwanghart & Jarmer, 2011; Zhu et al., 2014). It has been shown that topography plays a significant role in regulating the redistribution of light, heat, water, and sediments in mountainous terrains (Mvondo Owono et al., 2016; Patton et al., 2019). In addition, the topography is one of the main drivers of the spatial and temporal variation of SOC and N stocks and pedogenic processes in loess sediments (Fissore et al., 2017; He et al., 2021). The aspect slope can modify solar radiation intensity, functional diversity and biomass of fine roots, which are an important part of the soil carbon (Li et al., 2023a), and create microclimates that differ noticeably from regional climate conditions (Che et al., 2021; Zhu et al., 2017). Microclimates influence plant communities and species regarding slope aspects, increasing SOC variability at smaller scales. However, plant consist of an intricate combination of organic matter and mineral matter (He et al., 2023).

There is increasing concern regarding the substantial enrichment of OC and N in soil under different land uses (Wei et al., 2023). Response of ecosystem to land use change such as agriculture and horticulture has resulted in a change in the natural rate of carbon and nitrogen exchange between the atmosphere and the soil (Li & Shao, 2014; Zhang et al., 2023). Although the impacts of land use and management on topsoil SOC and N have been widely investigated, their influences as important drivers on subsoil SOC and N stocks are remarkably unknown. With the realization the importance of large qualities of OC stored in subsoils, interest has been growing in studying SOC dynamics not only in surface soils but further down the soil profile. In particular, the impact of agriculture and management practices on subsoils OC is a field of research interest.

The use of visible and near-infrared (Vis-NIR) spectroscopy has been identified as one of the promising alternatives to conventional methods of soil analysis. This method has demonstrated many advantages as a tool for determining soil organic carbon and nitrogen, including its speed, reliability, environmental friendliness, and affordability (Soriano-Disla et al., 2014). It has been argued that PLSR, because of its ability to deal with large data-sets, is the most accurate basis to determine soil properties (Khayamim et al., 2015). The PLSR algorithm coupled soil spectra has been frequently utilized to estimate soil organic carbon and nitrogen contents (Nawar et al., 2015; Sorenson et al., 2018; Yang et al., 2019). In recent decades, various data-mining approaches have been developed for estimating soil parameters based on soil spectra. It should be noted, however, that these methods focused mainly on spectroscopy and did not take into account the link between soil and the environmental data. Spectral data will produce more accurate and reliable estimates of soil properties when combined with environmental data due to the strong influence of topography factors and land use on soil properties. In the Zagros Mountains of western Iran, soils under various land uses are strongly influenced by topography. Therefore, as a result of topographic conditions, a variety of soil types are available with varying amounts of SOC and N. It is, however, not yet well understood how land use and topography affect soil OC and N stocks, particularly in the subsoil. Therefore, the aims of this study were to:

- Investigate the influence of topography features on soil organic carbon (OC) and nitrogen (N) stocks in both the topsoil and subsoil of a small calcareous watershed in the Zagros mountains of western Iran.
- Examine the impact of different land uses on the distribution of soil OC and N, considering the diverse soil types resulting from topographic conditions in the study area.
- Utilize VIS-NIR spectroscopy and remote sensing techniques to enhance the understanding of how land use and topography jointly affect OC and N stocks, particularly in the subsoil layer.

2. Materials and methods

2.1. Study area

The study site with an area of 1504 km^2 is located in the Southern Hamaden Province of Iran between 34°0′-34°30′ north latitude and 45°50′-48°30′ east latitude. It experiences a semi-humid climate, with an average annual precipitation of 317.0 mm and an average annual temperature of 11.5 °C. Summer temperatures are generally high (i.e. in June and July with an average of 23 °C) while winter temperatures are relatively low (i.e. from December to March with an average of 4 °C). According to the USDA Soil Taxonomy (USDA, 2010), the soils in the area are typically calcareous in nature, and commonly classified as Inceptisols, Entisols, Vertisols, and Alfisols (USDA, 2010). Most of the lands in the study area are used for agriculture. In addition to barley, wheat, and potatoes, privileged locations are also used for horticulture. The study site features diverse geological formations including narrow mountain ranges and intermountain depressions, shaped by deep-seated faults. Diverse geological features, such as magmatic rocks, evaporates, and turbidities, contribute to the complex geomorphic history. Miocene marine deposition, observed in formations adds to the intricate geomorphic tapestry shaped by ongoing tectonic processes (Afrasiabian et al., 2021).

2.2. Soil data

114 soil samples were collected from the soil surface layer within the study area, using a random sampling procedure, in order to provide a large distribution of samples throughout the study area (Fig. 1). There were three land uses from which the soil samples were collected, as follows: 40 samples were collected from agricultural land, 37 samples were collected from orchards, and 28 samples were collected from bare land. Additionally, the samples were grouped into four main aspects-slopes: the north aspect (27 samples), east aspect (28 samples), west aspect (30 samples), and south aspect (29 samples). A stainless-steel auger was used for soil sampling down to depth of 50 cm with three replicates. For bulk analysis, the samples were divided into two increments: topsoil

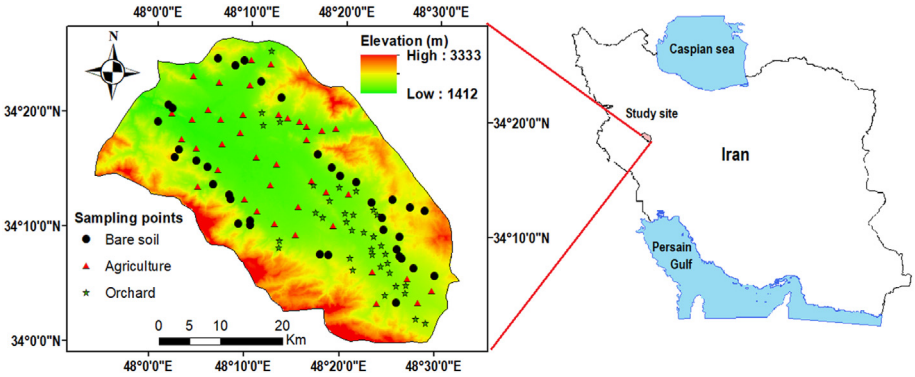

Fig. 1. Locations of the soil samples and the study site.

samples (a depth of 0–20 cm) and subsoil samples (a depth of 20–50 cm). Each increment's soil sample was homogenized and sent to the laboratory. The samples were air-dried, ground, and sieved before being analyzed to determine some of the general soil physicochemical properties. The soil bulk density (BD) of each soil depth interval was determined by dividing the mass of fine fractions (<2 mm) by the total volume of each increment. A hydrometer was used to determine soil texture. Soil organic matter was quantified using the Walkley-Black method, and total nitrogen was measured using the Kjeldahl method. The $CaCO_3$ concentration was determined with HCL 1 mol L^{-1} (Nelson & Sommers, 1996). A portable pH machine was used to measure soil pH.

2.3. Environment factors

In this study, we used 10 topographic attributes including elevation, slope (Fig. 2(a)), aspect (Fig. 2(b)), profile curvature (P_Cur), plan curvature (Pl_Cur), flow direction (FD), flow accumulation (FA), topographic wetness index (TWI) (Fig. 2(c)), length-slope factor (LS), stream power index (SPI) and sediment transport index (STI) (Fig. 2(d)), which have been used to determine soil erosion, sedimentation and redistribution (Table 1) (Liu et al., 2020). All topographic attributes were derived from a 30 × 30 m digital elevation model (DEM) provided by the United States Geological Survey (USGS) website. The USGS DEM was generated

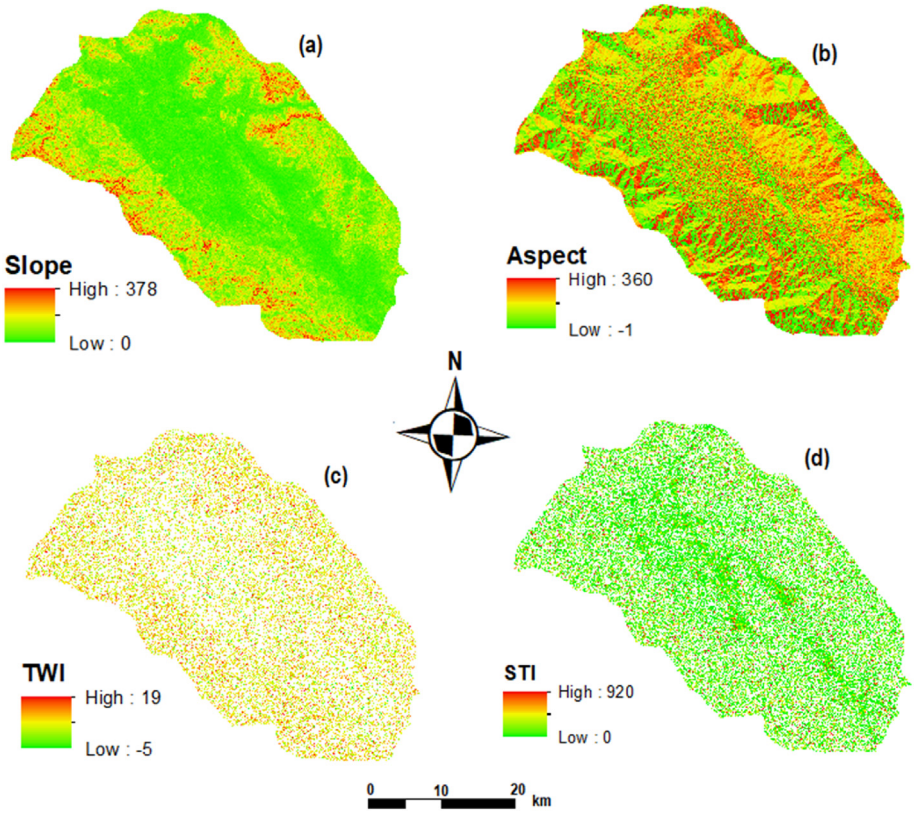

Fig. 2. Maps of the slope, aspect, TWI and STI. Slope was calculated based on the radiant.

Table 1
Definitions, formulas and significances of selected topographic factors.

Variables	Definition	Formula	Significance	References
Elevation (h)	Height from see level	–		
Slope (S) (radian)	An angle between a tangent and a horizontal planes at a given point	$S = arctan\sqrt{p^2+q^2}$	Velocity of runoff and soil-water content	Li and Shao (2014)
Aspect (A) (radian)	An angle clockwise from north to the horizontal projection of an external normal vector at a given point	$A = arctan\left(\frac{q}{p}\right)$	Soil-water balance, vegetation distribution	Barré et al. (2017)
Profile curvature (m^{-1})	Curvature of the surface in the direction of the steepest slope	$k_v = -\frac{p^2r+2pqs+p^2t}{(p^2+q^2)\sqrt{1+p^2+q^2}}$	Flow convergence and divergence, soil- water content	Troch et al. (2002)
Plan curvature	Curvature in a horizontal plane	$k_h = -\frac{q^2r+2pqs+q^2t}{(p^2+q^2)\sqrt{1+p^2+q^2}}$	Flow convergence and divergence, soil water content	Troch et al. (2002)
Catchment area (m^2)	Area draining to the catchment outlet	–	Runoff velocity and volume	(Moore et al., 1991; Tucker & Bras, 1998)
Flow accumulation (FA)	Upslope number of grid cells	–	Soil-water content and runoff volume	Mirzaee et al. (2017)
Topographic wetness index (TWI)	Frequencies and duration of saturated conditions	$TWI = \ln\left(\frac{A_S}{S}\right)$	Soil moisture distribution	Wilson and Gallant (2000)
Length-Slope factor (LS)	Erosive power of the terrain	$LS = (n+1)STI = \left(\frac{A_S}{22.13}\right)^{0.4}\left(\frac{\sin S}{0.0896}\right)^{1.3}$		Moore et al. (1991)
Stream power index (SPI)	Erosive power of overland flow	$SPI = A_s \tan\theta$	Soil erosion, convergence of flow	(Mirzaee et al., 2017; Wilson & Gallant, 2000)
Sediment transport index (STI)	Soil-water content and sediment transport	$STI = \left(\frac{A_S}{22.13}\right)^{0.4}\left(\frac{\sin S}{0.0896}\right)^{1.3}$	Soil erosion and deposition	(Mirzaee et al., 2017; Wilson & Gallant, 2000)
Where p, q, r, and t are partial derivatives of elevation (h): $h = f(x,y); p = \frac{\delta h}{\delta x}; q = \frac{\delta h}{\delta y}; r = \frac{\delta^2 h}{\delta x^2}; t = \frac{\delta^2 h}{\delta y^2}$				

radar sensors on the Sentinel-2 satellite (U.S. Geological Survey, 2021). Aspect, slope, and elevation maps were created in ArcMap v.10.6.2. Curvature metrics (P_Cur and Pl_Cur) were calculated using the slope and aspect modules of the System for Automated Geoscientific Analysis (SAGA) v. 2.2.5. The SPI and LS-factor modules in SAGA were used to generate stream power index and length-slope factor, respectively. Catchment area (m^2) and TWI were generated with the SAGA Wetness Index module. Flow direction and flow accumulation maps were extracted from the filtered DEM in ArcMap v.10.6.2. A Landsat Jun 8, 2021 with a resolution of 30 m was acquired from the USGS (U.S. Geological Survey, 2021) in order to generate the normalized difference vegetation index (NDVI) map, which is calculated as follows:

$$NDVI = \frac{NIR - RED}{NIR + RED} \quad (1)$$

where NIR represents the near-infrared reflectance band and Red represents the Red band. The mean NDVI value was 0.21, ranging from −0.15 to 0.57 (Fig. 3).

2.4. Spectroscopy

Approximately 50 g of sieved soil samples were illuminated under the camera obscura using a 50 W halogen lamp at an incidence angle of 45° and at a distance of around 50 cm from the surface of the sample. FieldSpec spectroradiometers was used to measure spectral reflectance (350–2500 nm) of soil samples (FieldSpec 3, Analytical Spectral Device, ASD Inc.) with 1 nm accuracy. A mean of 20 spectra was considered when measuring white reflectance every 5 min. To advance the spectra linearity, log (1/reflectance) was utilized to convert reflectance to absorbance. The noise in the spectra was reduced using Savitzky-Golay method via two smoothing filters and second-order polynomial approximation (Savitzky & Golay, 1964). By utilizing the whole spectrum, Unscrambler X v. 10.0 Software (CAMO AS, Oslo, Norway) constructed relationships between pre-processed spectra with SOC and TN content. Cross-validation was applied to determine b-coefficients between the content of SOC and TN and their spectra.

2.5. Statistical analysis

Data analyses were conducted using Statistica 8.0. Graphs were generated using Excel 2016. A Kolmogorov–Smirnov test

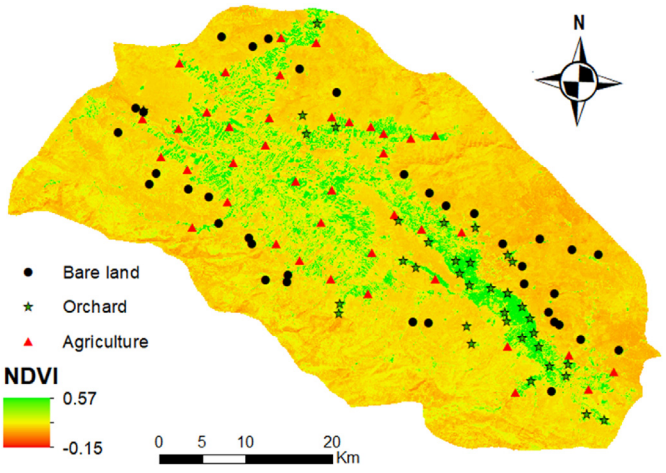

Fig. 3. NDVI map.

was performed to assess the normality of the data, determining whether any univariate parameters distribution among the different aspects and land uses deviated significantly from the norm. A one-way ANOVA was used to test the effects of land uses and aspects on SOC and TN stocks. A Tukey Honestly Significant Difference (HSD) test was conducted to compare multiple groups means. SOC and TN were also examined at both topsoil and subsoil using principal component analysis (PCA) on topographical attributes. Covariance matrices were used to calculate principal components and loading values. A forward stepwise multiple linear regression model was developed with terrain attributes at three depths to analyze the relationship between SOC and TN stocks. Furthermore, a Pearson correlation matrix was examined to evaluate the relationship between topsoil and subsoil OC and TN stocks at two depths with topography terrain attributes. Heatmap correlation graph was produced in the R software. The correlation heatmap takes this matrix and represents it visually using colors. Each cell in the heatmap corresponds to the correlation between two variables. The color of the cell indicates the strength and direction of the correlation. The following statistical indicators were used to evaluate the models' performance: R^2, RMSE (root mean square error), ME (mean error), and RPD ratio (predicted deviation):

$$R^2 = 1 - \frac{SSE}{SST} \quad (1)$$

$$RMSE = \sqrt{\left(\frac{\sum_{i=1}^{n}(P_i - O_i)^2}{n}\right)} \quad (2)$$

$$ME = \frac{\sum_{i=1}^{n}(P_i - O_i)}{n} \quad (3)$$

$$\mathrm{RPD} = \frac{STD}{\mathrm{RMSE}} \quad (4)$$

where n is the number of observations, O is the observed value, P is the predicted value, and STD and SEP are the standard deviations of the ground truth data and the standard errors of prediction. Viscarra-Rossel (2007) suggested that the prediction can be classified into: "excellent" class (RPD $\geq$2.5 and $R^2 \geq 0.80$), "good" class (RPD 2–2.5 and $R^2 \geq 0.70$), "moderate" class (RPD 1.5–2 and R2 $\geq$ 0.60) and "poor" class (RPD <1.5 and $R^2 < 0.60$).

3. Results and discussions

3.1. Soil properties

A description of the soil properties under three land uses is provided in Table 2. A mean pH > 7.5 indicates that soils are calcareous and alkaline, which could be caused by high soil $CaCO_3$ content (mean $CaCO_3$ = 44.9 %; Table 1). There is a wide range of soil particle proportions in the studied area, with clay ranging from 8.4 to 56.2%, sand from 5.5 to 66.4%, and silt from 15.4 to 66.3 %. Soils under agriculture and orchard have a higher mean clay content compared with soils under bare land. The most variable factor was clay with a CV value of 33.1%. Topsoil OC (3.9 kg m^{-2}) and TN (2.0 kg m^{-2}) stocks in orchard land use were higher than those in agriculture and bare land. Similarly, subsoil C and TN in the orchard were higher than those in agriculture and bare land. Additionally, both subsoil and topsoil C and T in agriculture were higher than bare land; however, the differences were insignificant.

3.2. Land use effect on SOC and TN

As shown in Fig. 4(a) and (b), soils under the orchard had higher topsoil and subsoil OC and TN stocks, followed by agriculture. In Fig. 4, boxplots shows that SOC and TN stocks in orchard are significantly larger than both agriculture and bare land; however, there was no significant differences between agriculture and bare land. Soils under orchards had the largest SOC (7.4 kg m^{-2}) and TN (2.4 kg m^{-2})) stocks (0–50 cm) among the three land uses, followed by soils under agriculture. There were significant differences between OC and TN stocks between the orchard and bare land; however, the difference between agriculture and bare land was insignificant. According to Gregory et al. (2014), agricultural soils had significantly lower SOC stocks than soils under orchards. In orchards, high-ground litter and intensive fine roots are large sources of C input to the soil profile. Similarly, cropped soils generally have a larger density than native soils, which directly impacts the soil porosity and indirectly affects SOC distribution by effects on illuviation and percolation processes, faunal activities and root systems. Converting grassland to agricultural land releases SOC, and following land use changes in the opposite direction accumulates SOC content. In addition, the application of livestock manure for soil improvement can increase the OC in agricultural

Table 2
A summary of soil properties under three land uses. STD is standard deviation, and CV is coefficient variation.

Parameter		pH	BD	Sand	Clay	Silt	$CaCO_3$	Topsoil C	Subsoil C	Topsoil TN	Subsoil TN	Topsoil C	Subsoil C stocks	Topsoil TN stocks	Subsoil TN stocks
Unit		–	(g cm^{-3})	(%)	(%)	(%)	(%)	(%)	(%)	(%)	(%)	(kg m^{-2})	(kg m^{-2})	(kg m^{-2})	(kg m^{-2})
Agriculture	Min	7.2	1.2	5.5	8.4	15.4	11.5	0.6	0.3	0.2	0.1	1.8	1.0	0.4	0.1
	Max	8.4	1.8	66.4	54.3	66.3	66.5	1.6	1.4	0.9	0.5	4.7	4.4	2.8	0.6
	Average	7.8	1.5	28.0	30.6	41.4	44.8	1.1	0.9	0.5	0.2	3.1	2.8	1.4	0.3
	STD	0.3	0.1	19.7	12.0	12.4	11.6	0.2	0.2	0.2	0.1	0.5	0.6	0.6	0.1
	CV	4.2	8.8	30.4	39.3	29.9	25.8	18.1	24.2	41.3	28.8	17.0	23.2	39.9	48.5
Orchard	Min	7.0	1.0	0.9	8.5	19.6	11.5	1.0	0.8	0.2	0.1	2.5	2.2	0.5	0.1
	Max	8.4	1.6	68.9	49.6	75.6	66.5	2.6	2.4	1.4	0.7	6.6	6.8	3.9	1.0
	Average	7.8	1.3	29.4	30.4	40.1	44.1	1.5	1.2	0.7	0.3	3.9	3.5	2.0	0.4
	STD	0.3	0.1	17.3	9.9	12.7	11.7	0.3	0.3	0.3	0.2	0.9	0.9	0.8	0.2
	CV	4.1	9.0	18.9	32.4	31.5	26.6	24.0	26.1	39.8	49.1	23.9	26.5	21.3	28.6
Bare land	Min	7.3	1.1	2.6	5.1	8.8	17.5	0.49	0.26	0.1	0.0	1.2	0.6	0.3	0.1
	Max	8.5	1.9	86.1	48.4	73.4	64.5	1.66	1.42	0.9	0.3	4.3	3.7	2.7	0.4
	Average	7.8	1.5	34.1	20.7	45.2	44.4	0.82	0.60	0.4	0.1	2.4	1.8	1.1	0.2
	STD	0.3	0.2	23.4	10.2	18.4	11.5	0.24	0.23	0.2	0.1	0.8	0.7	0.7	0.1
	CV	4.3	12.5	28.7	29.1	20.7	25.8	29.43	39.20	23.4	27.9	32.0	29.6	32.5	31.6

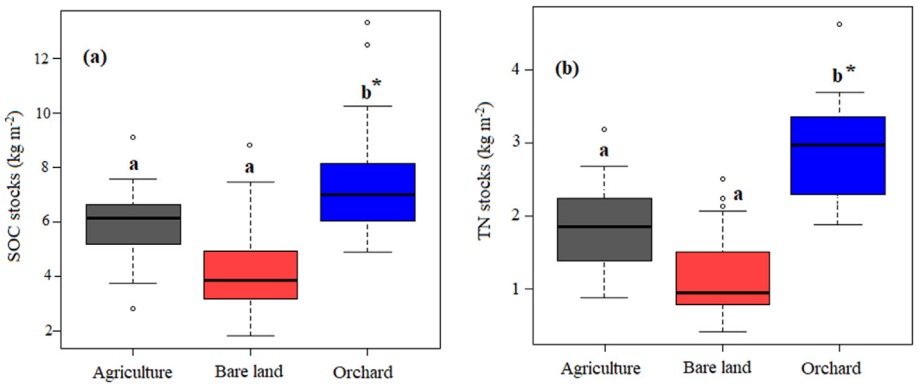

Fig. 4. Mean SOC and TN stocks (kg m^{-2}) in under different land uses. * shows the significant levels at 0.95 ($p < 0.05$). The same letter show no significant difference between the land uses. Different letters indicate significant difference between the land uses.

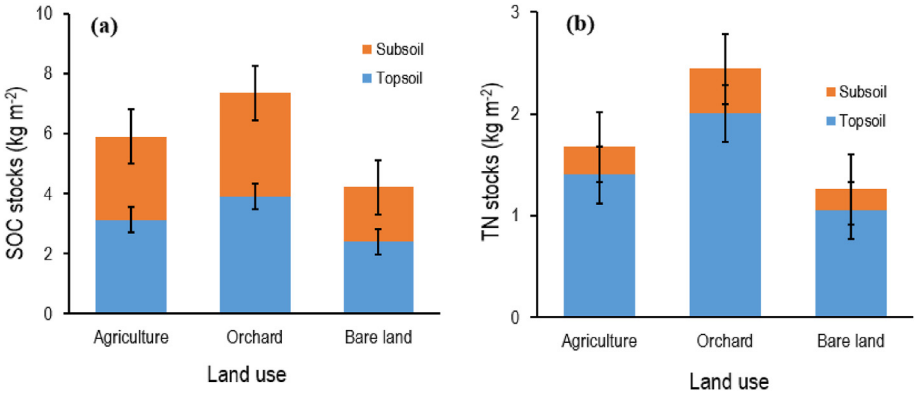

Fig. 5. SOC and TN stocks (kg m^{-2}) in topsoil (0–20 cm) and subsoil (20–50 cm) under different land uses.

soil (Zhang et al., 2020; Zhang et al., 2021).

Almost 50% of the SOC stocks belong to subsoils for three land uses (Fig. 5(a) and (b)). However, more than 70% of TN stocks are stored in topsoil. It is worth mentioning that the large quantities of SOC and TN stocks in subsoils under all land use (Fig. 4) indicate a considerable underestimation of SOC and TN stocks if particularly SOC stocks are determined only at the shallower depths. This might be due to the fact that topsoil receives more nitrogen from different sources (fertilizer or nitrogen fixation by plants) compared to subsoils. The general narrative reason for high subsoil OC stocks in this mountainous region is that low temperature and high precipitation restrain the decomposition of SOC and lead to SOC accumulation in high-elevation areas (Baumgarten et al., 2021). These findings align with the results by Patton et al. (2019) and Lozano-García et al. (2016) who found 51% and 41% of the total SOC stocks below 30 and 25 cm, respectively. Wiesmeier et al. (2013) also reported a considerable amount of SOC stocks (20–47%) in the subsoil of Germany. Yimer et al. (2006) and Lozano-García et al. (2016) also reported that 41% and 51% of TN stocks at a depth of 0–25 cm. Bangroo et al. (2017) also pointed out a similar range of TN stocks for 0–20 cm (59–62%) and for 20–60 cm (41-38%) in the Himalayan forest.

3.3. Aspect effect on SOC and TN

The sampling sites are classified into four main aspects:North (N), South (S), West (W), and East (E). Fig. 6 illustrates the average SOC and TN stocks for all aspects. The aspect influences microclimates and vegetation intensity, resulting in significant variation in SOC stocks (Che et al., 2021; Sun et al., 2015; Zhu et al., 2017). The SOC and TN stocks in the S aspects were significantly larger than those in other aspects, particularly in the N aspects. However, the difference between S and W aspects was insignificant (Fig. 6).

SOC and TN stocks were exceeded in shaded as well as semi-shaded areas (S and SW aspects). Due to stronger solar radiation and higher evaporation, sunny slopes (N and E aspects) retain less soil water content. Bangroo et al. (2017) reported that soil N mineralization and decomposition rates were higher in the south-facing aspect than those in the north-facing. This could be due to the influence of aspect on solar radiation and soil water content. As aforementioned, the solar radiation received in north-facing aspects (S and SW aspects) is low, which affects microbial activities (Fairbanks et al., 2020; Xue et al., 2018) due to changing soil water content and temperature. In addition, the chemical properties of soil may lead to the fractionation of hydrogen and oxygen in soil water (Zhou & Yang, 2023; Zhu et al., 2022) that affect soil organic carbon. Consequently, there is a significant decrease in SOC and N losses in S aspects owing to a longer resistance time for the litter decomposition (Bangroo et al., 2017). Patton et al. (2019) pointed out that SOC stocks were about three times larger in north-facing aspects compared to south-facing aspects. According to Zhu et al. (2017), SOC content increased from the south-facing aspect to the north-facing aspect over a soil profile at each depth. Differences in hydrological and received solar energy linked to aspect may induce the divergence in vegetation intensity, soil formation and SOM decomposition. These leads to locally variation of temperature and precipitation, which are major regulators of SOM decomposition rates as soil microbe communities can be highly sensitive to

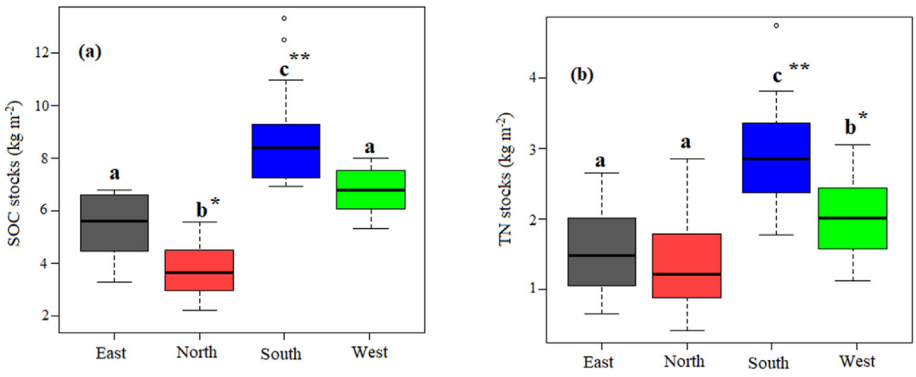

Fig. 6. Mean SOC and TN stocks (kg m^{-2}) in under slope aspects. * and ** show the significant levels at 0.95 ($p < 0.05$) and 0.99 ($p < 0.01$), respectively. The same letter show no significant difference between the land uses. Different letters indicate significant difference between the land uses.

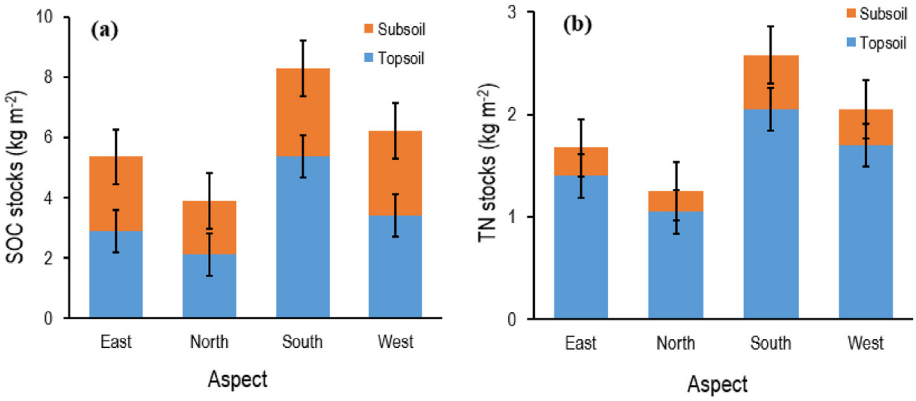

Fig. 7. SOC and TN stocks (kg m^{-2}) in topsoil (0–20 cm) and subsoil (20–50 cm) under different land uses.

temperature changes (Jia et al., 2017). Moreover, vegetation intensity increased from N (mean NDVI = 0.27) to S aspects (mean NDVI = 0.48), indicating a higher density of vegetation in S and W aspects at the study site, where organic matter previously locked in frozen soils may be released into the atmosphere (Luo et al., 2022). Due to this, soils with lower vegetation on the north and possibly east aspects are more likely to experience runoff, which can result in the loss of SOC.

In both depth intervals, there was a similar pattern of decreasing SOC stocks along the soil profile associated with different aspects (Fig. 7(a) and (b)). It is similar to the findings of Sun et al. (2015), Li and Shao (2014), Zhu et al. (2017), and Fairbanks et al. (2020). Topsoil (0–20 cm) accounted for 50% of SOC and TN stocks in all aspects. TN and SOC stocks of topsoil (Fig. 2(a)) are not significantly different in all respects. There was no difference between topsoil and subsoil in SOC stocks except in S. However, there was a significant difference between topsoil and subsoil in TN stocks, especially in S and W. Bangroo et al. (2017) reported that soil N mineralization and decomposition rates were higher in the south-facing aspect than those in the north-facing. This influence could be due to the aspects on solar radiation and soil water content. As aforementioned, the solar radiation received in north-facing aspects (S and SW aspects) is low, which affects microbial activities (Fairbanks et al., 2020; Mvondo et al., 2016; Xue et al., 2018) due to changing soil water content and temperature. Consequently, there is a significant decrease in SOC and N losses in S aspects owing to a longer resistance time for the litter decomposition (Bangroo et al., 2017).

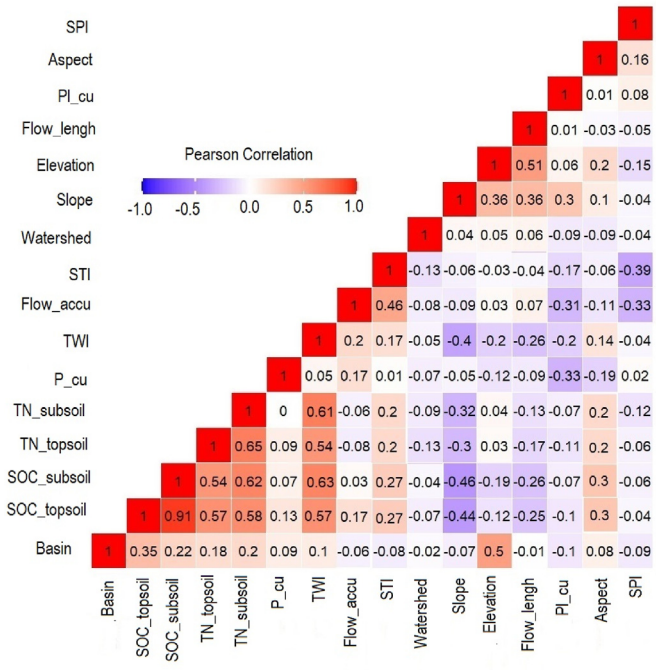

Fig. 8. Correlation matrix of SOC and TC stocks at different depths with topographic terrain attributes.

3.4. Topography terrain attributes

Fig. 8 indicates the Pearson correlation used to analyze the relationship between terrain attributes and the stocks of SOC and TN at two depths. The correlations between terrain attributes and SOC stocks were generally greater than those between terrain attributes and TN stocks. There was a strong interrelationship between many topographic attributes, which cannot be considered independent variables. A significant relationship was found between the variables TWI, aspect, FA, and STI. Therefore, PCA was used to identify the major variables controlling SOC and TN stocks. Table 2 lists the first four PCA components responsible for 74% of the variability in topographic attributes. TWI, Slope, P_CU, FL, and LS-factor were the most significant terrain attributes for PC1 (Table 3). Elevation, SPI, and FA aspects contributed to PC2. In a study by Wiesmeier et al. (2013), TWI and elevation were found as the main controlling factors of SOC and TN stocks in grasslands in Germany. TWI was also identified as the second major predictor variable for SOC stocks estimation in Germany's topsoil and subsoil by Mayer et al. (2019). Even though elevation in PC2 had a loading score of −0.619, it was not significantly correlated with either SOC or TN stocks at all depths (Fig. 8), indicating that elevation likely did not influence soil erosion and deposition. It might be due to the fact that the samples were collected at relatively similar altitudes. A negative correlation was found between slope and FL with SOC and TN stocks in topsoil and subsoil (Fig. 8), whereas several attributes (i.e., STI, TWI, and aspect) were significantly positively correlated with SOC stocks ($p < 0.05$). The slope had a significantly negative correlation with TN stocks, whereas the TWI and FD of the soil had a significant positive correlation, particularly in deeper soil layers.

TWI exhibited the strongest positive correlation with SOC stocks (0.57−0.63) as well as TN stocks (0.54−0.61) along the soil depth (Fig. 8), which is consistent with the findings of Li et al. (2018), who cited TWI as the most significant terrain attribute impacting SOC stocks. TWI has also been identified as the second most important variable affecting SOC distribution in permafrost by Siewert (2018). Recent research by Fairbanks et al. (2020) indicates that NDVI, clay content, and TWI are fundamentally involved in biochemical cycling in complex landscapes. Mayer et al. (2019) reported a significant positive correlation of 0.29 and 0.32 between topsoil and subsoil OC stocks with TWI, respectively. In addition to identifying inundated areas, the TWI is an effective attribute for investigating soil-water content spatial variation along the slope (Li et al., 2018; Liu et al., 2020). TWI is used to determine soil moisture gradients. Positive relationships between TWI and SOC and TN stocks showed that SOC and TN contents tend to accumulate in areas with a high TWI where soil moisture is higher. A significant increase in SOC and TN in soils with a high soil-water content results from increased plant production and a decrease in soil organic matter decomposition (Li et al., 2018; Li et al., 2023b; Pei et al., 2010). Generally, high TWI values were found at lower elevations of the landscape in our study. High TWI references high soil water content responsible for SOM accumulation in the subsoil (Wiesmeier et al., 2013). The spatial heterogeneity of subsoil OC stocks is therefore controlled by the lateral transport of OC by erosion to lowland positions with potentially saturated soil identified by a high TWI (Mayer et al., 2019).

Table 3
Variable loadings in the principal components (PCs) for topographic factors.

	PC1 (34%)	PC2 (16%)	PC3 (14%)	PC4 (10%)
Elevation	−0.367	−0.619	0.395	−0.020
Slope	−0.667	−0.266	−0.262	0.021
Aspect	−0.200	0.069	0.535	0.478
Flow_lengh	−0.510	−0.511	−0.130	−0.140
Flow_accu	0.495	−0.600	−0.142	0.076
Watershed	−0.123	−0.001	−0.059	−0.377
Pl_cu	−0.530	0.265	−0.243	0.415
P_cu	0.361	−0.099	0.043	−0.642
Basin	−0.085	−0.345	0.735	−0.162
STI/LS	0.447	−0.525	−0.277	0.385
SPI	−0.207	0.624	0.226	−0.175
TWI	0.689	0.053	0.411	0.294

3.5. Soil spectra analysis

It can be seen in Fig. 9 that there are two distinct shoulders around the wavelengths 600−700 nm. Additionally, there are four definite shoulders at 1414, 1915, 2212, and 2341 nm. There is evidence that soil organic carbon can affect spectral data that range from 700 nm to 2450 nm, according to Stenberg (2010). Tahmasbian et al. (2018) also reported that the important wavelengths for the prediction of TC and TN were mainly observed in the spectral regions of 740−800 and 900-100 nm, respectively. Additionally, there are a number of specific absorption features around the wavelength of 950 nm, as well as between the wavelengths of 2300−2400 nm. It is also possible to see some absorption features in the near 950 nm as well as between 2300 and 2400 nm in the near 950 nm range. There is a high percentage of calcareous soils in this study, which suggests that the absorption peaks near 2340 nm may be attributed to the presence of CO32- groups in carbonates (mainly calcite), which is consistent with previous research (Babaeian et al. 2015).

The average of the soil spectra for three land uses (orchard, agriculture, bare land) is shown in Fig. 9(a). The orchard with higher OC content in both topsoil and subsoil had the lowest spectra, followed by agricultural and bare lands. Salehi-Varnousfaderani et al. (2022) and Ostovari et al. (2018) also reported the effect of land use on soil spectra. Soil organic matter, which can be significantly affected by land use, is a vital soil property influencing the soil spectra due to its influence on the color of the soil. Therefore, soil spectra are affected by changes in land use, which have profound effects on soil organic matter (Ostovari et al., 2018). The highest soil spectra in the bare lands could be due to that bare soils are mainly found at high altitudes where the soil is more prone to erosion due to lower vegetation cover.

Fig. 9(b) shows the mean spectra of the soil samples situated on the four main aspects of topography. As given in Fig. 9(b), the N aspects (south-facing aspects) had the highest soil spectra compared to other aspects. In contrast, the S aspects (north-facing aspects) had the soil spectra. Generally, soils in the S and W aspects had a higher water content than N and E aspects. This can reduce soil temperature, consequently reducing microbial activities, as a result, and a decrease decomposition of soil organic matter. SOC distribution patterns might contribute to the differences in land cover along the different aspects. There is an increased risk of erosion and degradation in areas with lower-cover vegetation, which can result in SOC distribution. As depicted in Fig. 9(c), topsoil had lower spectra than subsoil. This may be becausetopsoils are generally darker than subsoil because of having larger soil organic matter stocks which come from different sources including root litter and exudates, plant residues, roots, and ground litter.

Fig. 10 shows the topsoil and measured subsoil OC and TN contents versus the predicted OC and TN using PLSR and soil spectra. In both the calibration and validation datasets, there is a good distribution of SOC and TN around the 1:1 lines (Fig. 10). This indicates the PLSR model predicts OC and TN with a high degree of accuracy. As provided in Table 4, the PLSR showed a better performance for the topsoil OC and TN compared with the subsoil OC

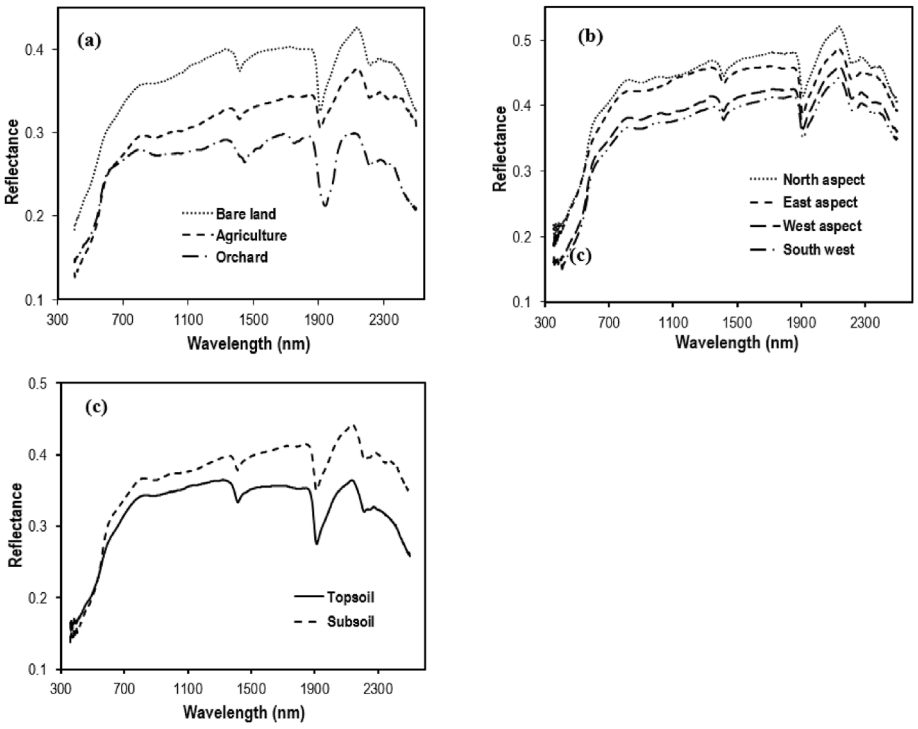

Fig. 9. Soil spectral reflectance under (a) three soil land uses, (b) different aspects and soil profiles.

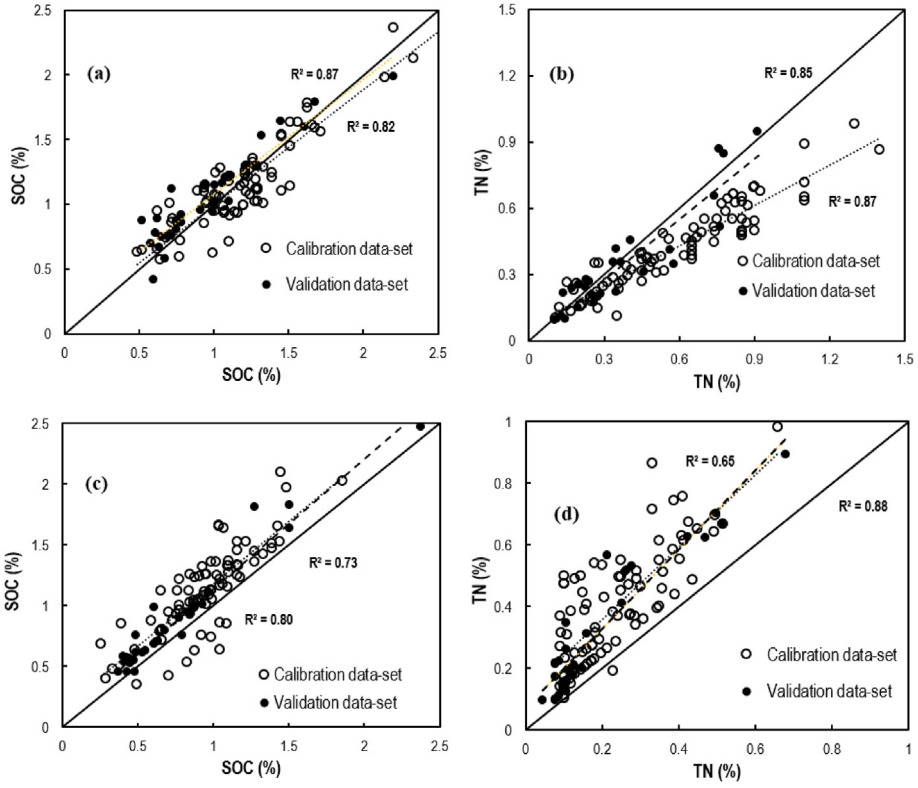

Fig. 10. Scatter plots for the prediction of topsoil OC (a), subsoil OC (b), topsoil TN (c) and subsoil (d) contents using the PLSR model and soil spectra.

and TN contents in both calibration and validation data sets. This can be associated with higher OC and TN concentrations in the topsoil that has higher reflectance. For topsoil, the PLSR with R^2 = 0.82, RMSE = 0.15 %, and RPD ratio = 2.7 and R^2 = 0.82, RMSE = −0.21 %, and RPD ratio = 2.4 showed an excellent and good prediction for OC and TN content, respectively (Table 4) (Viscarra-

Table 4
Statistical indices for the PLSR method for topsoil and subsoil OC and TN prediction using soil spectra.

Methods	R^2		RMSE %		ME %		RPD
	Validation	Calibration	Validation	Calibration	Validation	Calibration	
Topsoil OC	0.87	0.82	0.16	0.15	0.030	−0.02	2.7
Subsoil OC	0.73	0.80	0.51	0.90	0.12	0.18	2.3
Topsoil TN	0.85	0.87	0.10	0.21	−0.16	−0.01	2.4
Subsoil TN	0.88	0.65	0.38	0.43	0.16	0.12	2.2

Rossel, 2007). Tahmasbian et al. (2018) showed the advanced models had an acceptable performance with high R^2 and low RMSE in the prediction of soil carbon and nitrogen and their isotope compositions. Yang et al. (2019) also pointed out the high efficiency of the PLSR model for predicting SOC. It is worth mentioning that the PLSR model slightly underestimated the topsoil and subsoil OC and TN content; while it shows an overestimation for both subsoil OC and TN contents, particularly for TN content. Ding et al. (2018) highlighted that the combination of VIS-NIR spectroscopy technique and the PLSR model could provide a fast, economical, and robust approach to monitoring, detect, and estimate SOC content. Sorenson et al. (2018) indicated that VIS-NIR spectroscopy combined with could be applied to characterize the spatial variability of SOC and TN at the soil aggregate scales.

4. Conclusion

The goal of the current study was to employ VIS-NIR soil spectral and environmental data together with the Partial least-squares-regression (PLSR) model to examine the impact of topography features and land use on topsoil and subsoil OC and TN stocks. The results showed that the biggest SOC (7.4 kg m^{-2}) stocks were found in soils (0–50 cm) used for orchards and that the largest TN (2.4 kg m^{-2}) stocks were found orchards soils. Because the soils on the south aspects have a higher soil-water content and lower temperature, which results in a decrease in soil organic matter decomposition, their OC stocks (8.3 kg m^{-2}) were significantly higher than those of soils located on other aspects, particularly the north aspects (3.9 kg m^{-2}). The topographical wetness index had the greatest loading score among the terrain variables, showed the strongest positive connection with SOC stocks (0.57–0.63) and TN stocks (0.54–0.61), and indicated the key topographic feature regulating SOC stocks, particularly in the subsurface. Additionally, our findings demonstrated that, as compared to other aspects, soils on the N aspects (south-facing aspects) had the highest spectra. The outcomes also showed that the PLSR had excellent prediction for OC content, with R2 = 0.82, RMSE = 0.15%, and RPD. We concluded that the PLSR)model, demonstrates a remarkable capability to accurately forecast the organic carbon (OC) and nitrogen (N) content in both topsoil and subsoil across various aspect slopes. This finding underscores the versatility and robustness of the PLSR model in conjunction with Vis-NIR spectroscopy, showcasing its potential as a reliable tool for predicting soil organic carbon and nitrogen in diverse geographical conditions.

Funding

This work was supported by The National Natural Science Foundation of China (No.41830643), The National Science and Technology Basic Resources Survey Project (No. 2019FY101703) and The Higher Education Discipline Innovation Project (D18012).

CRediT authorship contribution statement

Jingrong Zhu: Writing – original draft, Methodology, Investigation, Formal analysis, Data curation. **Yihua Jin:** Writing – original draft, Resources, Data curation, Conceptualization. **Weihong Zhu:** Validation, Software, Investigation, Conceptualization. **Dong Kun Lee:** Writing – original draft, Visualization, Validation, Supervision, Conceptualization.

Declaration of competing interest

The authors declare that they have no known competing financial interests or personal relationships that could have appeared to influence the work reported in this paper.

References

Adhikari, K., & Hartemink, A. E. (2016). Linking soils to ecosystem services — a global review. *Geoderma, 262*, 101–111. https://doi.org/10.1016/j.geoderma.2015.08.009

Afrasiabian, A., Mahmoudi Sivand, S., Dogančić, D., Plantak, L., & Đurin, B. (2021). Geological features for geotourism in the zanjan and hamadan area, northern Iran. *Sustainability, 13*, 6587. https://doi.org/10.3390/su13126587

Alcántara, V., Don, A., Well, R., & Nieder, R. (2016). Deep ploughing increases agricultural soil organic matter stocks. *Global Change Biology, 22*(8), 2939–2956. https://doi.org/10.1111/gcb.13289

Babaeian, E., Homaee, M., Carsten Montzka, C., Vereecken, H., & Ali Norouzi, A. A. (2015). Towards retrieving soil HydraulicProperties by hyperspectral remote sensing. *Vadose Zone Journal*. https://doi.org/10.2136/vzj2014.07.0080

Bangroo, S. A., Najar, G. R., & Rasool, A. (2017). Effect of altitude and aspect on soil organic carbon and nitrogen stocks in the Himalayan Mawer Forest Range. *Catena, 158*, 63–68. https://doi.org/10.1016/j.catena.2017.06.017

Barré, P., Durand, H., Chenu, C., Meunier, P., Montagne, D., Castel, G., Billiou, D., Soucémarianadin, L., & Cécillon, L. (2017). Geological control of soil organic carbon and nitrogen stocks at the landscape scale. *Geoderma, 285*, 50–56. https://doi.org/10.1016/j.geoderma.2016.09.029

Batjes, N. H. (2014). Total carbon and nitrogen in the soils of the world. *European Journal of Soil Science, 65*(1), 10–21. https://doi.org/10.1111/ejss.12114_2

Baumgarten, A., Haslmayr, H.-P., Schwarz, M., Huber, S., Weiss, P., Obersteiner, E., Aust, G., Englisch, M., Horvath, D., Leitgeb, E., Foldal, C., Rodlauer, C., Bohner, A., Spiegel, H., & Jandl, R. (2021). Organic soil carbon in Austria – status quo and foreseeable trends. *Geoderma, 402*, Article 115214. https://doi.org/10.1016/j.geoderma.2021.115214

Che, M., Gong, Y., Xu, M., Kang, C., Lv, C., He, S., & Zheng, J. (2021). Effects of elevation and slope aspect on the distribution of the soil organic carbon associated with Al and Fe mineral phases in alpine shrub-meadow soil. *The Science of the total environment, 753*, Article 141933. https://doi.org/10.1016/j.scitotenv.2020.141933

Ding, J., Yang, A., Wang, J., Sagan, V., & Yu, D. (2018). Machine-learning-based quantitative estimation of soil organic carbon content by VIS/NIR spectroscopy. *PeerJ, 6*, Article e5714. https://doi.org/10.7717/peerj.5714

Fairbanks, D., Shepard, C., Murphy, M., Rasmussen, C., Chorover, J., Rich, V., & Gallery, R. (2020). Depth and topographic controls on microbial activity in a recently burned sub-alpine catchment. *Soil Biology and Biochemistry, 148*, Article 107844. https://doi.org/10.1016/j.soilbio.2020.107844

Ferretti, C. G. (2019). Relationship between the geology, soil assessment, and terroir of gewürtztraminer vineyards: A case study in the dolomites of northern Italy. *Catena, 179*, 74–84. https://doi.org/10.1016/j.catena.2019.03.044

Fissore, C., Dalzell, B. J., Berhe, A. A., Voegtle, M., Evans, M., & Wu, A. (2017). Influence of topography on soil organic carbon dynamics in a Southern California grassland. *Catena, 149*, 140–149. https://doi.org/10.1016/j.catena.2016.09.016

He, M., Dong, J., Jin, Z., Liu, C., Xiao, J., Zhang, F., & Deng, L. (2021). Pedogenic processes in loess-paleosol sediments: Clues from Li isotopes of leachate in Luochuan loess. *Geochimica et Cosmochimica Acta, 299*, 151–162. https://doi.org/10.1016/j.gca.2021.02.021

He, M., Ren, T., Jin, Z. D., Deng, L., Liu, H., Cheng, Y. Y., & Chang, H. (2023). Precise analysis of potassium isotopic composition in plant materials by multi-collector inductively coupled plasma mass spectrometry. *Spectrochimica Acta Part B: Atomic Spectroscopy, 209*, Article 106781. https://doi.org/10.1016/j.sab.2023.106781

Jia, J., Feng, X., He, J.-S., He, H., Lin, L., & Liu, Z. (2017). Comparing microbial carbon sequestration and priming in the subsoil versus topsoil of a Qinghai-Tibetan

alpine grassland. *Soil Biology and Biochemistry, 104*, 141–151. https://doi.org/10.1016/j.soilbio.2016.10.018

Jia, B., & Zhou, G. (2023). Estimation of global karst carbon sink from 1950s to 2050s using response surface methodology. *Geo-spatial Information Science*. https://doi.org/10.1080/10095020.2023.2165974

Khayamim, F., Wetterlind, J., Khademi, H., Robertson, J., Canod, A., & Stenberg, B. (2015). Using visible and near infrared spectroscopy to estimate carbonates and gypsum in soils in arid and subhumid regions of Isfahan, Iran. *Journal of Near Infrared Spectroscopy, 23*, 155–165.

Li, D., & Shao, M. (2014). Soil organic carbon and influencing factors in different landscapes in an arid region of northwestern China. *CATENA, 116*, 95–104. https://doi.org/10.1016/j.catena.2013.12.014

Li, X., McCarty, G. W., Karlen, D. L., & Cambardella, C. A. (2018). Topographic metric predictions of soil redistribution and organic carbon in Iowa cropland fields. *CATENA, 160*, 222–232. https://doi.org/10.1016/j.catena.2017.09.026

Li, W., Wang, C., Liu, H., Wang, W., Sun, R., Li, M., … Fu, S. (2023a). Fine root biomass and morphology in a temperate forest are influenced more by canopy water addition than by canopy nitrogen addition. *Frontiers in Ecology and Evolution, 11*. https://doi.org/10.3389/fevo.2023.1132248

Li, W., Wang, W., Sun, R., Li, M., Liu, H., Shi, Y., & Fu, S. (2023b). Influence of nitrogen addition on the functional diversity and biomass of fine roots in warm-temperate and subtropical forests. *Forest Ecology and Management, 545*, Article 121309. https://doi.org/10.1016/j.foreco.2023.121309

Liu, Y., Zhang, L., Lu, J., Chen, W., Wei, G., & Lin, Y. (2020). Topography affects the soil conditions and bacterial communities along a restoration gradient on Loess-Plateau. *Applied Soil Ecology, 150*, Article 103471. https://doi.org/10.1016/j.apsoil.2019.103471

Lozano-García, B., Parras-Alcántara, L., & Brevik, E. C. (2016). Impact of topographic aspect and vegetation (native and reforested areas) on soil organic carbon and nitrogen budgets in Mediterranean natural areas. *The Science of the total environment, 544*, 963–970. https://doi.org/10.1016/j.scitotenv.2015.12.022

Luo, J., Niu, F., Lin, Z., Liu, M., Yin, G., & Gao, Z. (2022). Abrupt increase in thermokarst lakes on the central Tibetan Plateau over the last 50 years. *Catena, 217*, Article 106497. https://doi.org/10.1016/j.catena.2022.106497

Matteodo, M., Grand, S., Sebag, D., Rowley, M., Vittoz, P., & Verrecchia, E. P. (2018). Decoupling of topsoil and subsoil controls on organic matter dynamics in the Swiss Alps. *Geoderma, 330*, 41–51. https://doi.org/10.1016/j.geoderma.2018.05.011

Mayer, S., Kühnel, A., Burmeister, J., Kögel-Knabner, I., & Wiesmeier, M. (2019). Controlling factors of organic carbon stocks in agricultural topsoils and subsoils of Bavaria. *Soil and Tillage Research, 192*, 22–32. https://doi.org/10.1016/j.still.2019.04.021

Mirzaee, S., Ghorbani-Dashtaki, S., Mohammadi, J., Asadzadeh, F., & Kerry, R. (2017). Modeling WEPP erodibility parameters in calcareous soils in northwest Iran. *Ecological Indicators, 74*, 302–310. https://doi.org/10.1016/j.ecolind.2016.11.040

Moore, I. D., Grayson, R. B., & Ladson, A. R. (1991). Digital terrain modelling: A review of hydrological, geomorphological, and biological applications. *Hydrological Processes, 5*(1), 3–30. https://doi.org/10.1002/hyp.3360050103

Mvondo, F., Ntamak-Nida, M.-J., Dauteuil, O., Guillocheau, F., & Njom, B. (2016). Morphology and long-term landscape evolution of the South African plateau in South Namibia. *Catena, 142*, 47–65. https://doi.org/10.1016/j.catena.2016.02.012

Nawar, S., Buddenbaum, H., & Hill, J. (2015). Estimation of soil salinity using three quantitative methods based on visible and near-infrared reflectance spectroscopy: A case study from Egypt. *Arabian Journal of Geosciences, 8*(7), 5127–5140.

Nelson, D. W., & Sommers, L. E. (1996). Total carbon, organic carbon, and organic matter. In D. L. Sparks, A. L. Page, P. A. Helmke, & R. H. Loeppert (Eds.), *Methods of soil analysis Part 3—chemical methods. SSSA book series* (pp. 961–1010). Madison, WI: Soil Science Society of America, American Society of Agronomy.

Osanai, Y., Knox, O., Nachimuthu, G., & Wilson, B. (2020). Increasing soil organic carbon with maize in cotton-based cropping systems: Mechanisms and potential. *Agriculture, Ecosystems & Environment, 299*, Article 106985. https://doi.org/10.1016/j.agee.2020.106985

Ostovari, Y., Ghorbani-Dashtaki, S., Bahrami, H. A., Abbasi, M., Dematte, J. A. M., Arthur, E., & Panagos, P. (2018). Towards prediction of soil erodibility, SOM and $CaCO_3$ using laboratory Vis-NIR spectra: A case study in a semi-arid region of Iran. *Geoderma, 314*, 102–112.

Patton, N. R., Lohse, K. A., Seyfried, M. S., Godsey, S. E., & Parsons, S. B. (2019). Topographic controls of soil organic carbon on soil-mantled landscapes. *Scientific Reports, 9*(1), 6390. https://doi.org/10.1038/s41598-019-42556-5. https://www.nature.com/articles/s41598-019-42556-5

Pei, T., Qin, C.-Z., Zhu, A.-X., Yang, L., Luo, M., Li, B., & Zhou, C. (2010). Mapping soil organic matter using the topographic wetness index: A comparative study based on different flow-direction algorithms and kriging methods. *Ecological Indicators, 10*(3), 610–619. https://doi.org/10.1016/j.ecolind.2009.10.005

Qiu, D., Zhu, G., Bhat, M. A., Wang, L., Liu, Y., Sang, & Sun, N. (2023). Water use strategy of nitraria tangutorum shrubs in ecological water delivery area of the lower inland river: Based on stable isotope data. *Journal of Hydrology, 624*, Article 129918. https://doi.org/10.1016/j.jhydrol.2023.129918

Salehi-Varnousfaderani, B., Afshin Honarbakhsh, A., Tahmoures, M., & Akbari, M. (2022). Soil erodibility prediction by Vis-NIR spectra and environmental covariates coupled with GIS, regression and PLSR in a watershed scale, Iran. *Geoderma Regional, 28*, Article e00470. https://doi.org/10.1016/j.geodrs.2021.e00470, 2022.

Savitzky, A., & Golay, J. J. E. (1964). Smoothing and differentiation of data by simplified least squares procedures. *Analytical Chemistry, 36*(8), 1627–1639.

Schwanghart, W., & Jarmer, T. (2011). Linking spatial patterns of soil organic carbon to topography — a case study from south-eastern Spain. *Geomorphology, 126*(1–2), 252–263. https://doi.org/10.1016/j.geomorph.2010.11.008

Siewert, M. B. (2018). High-resolution digital mapping of soil organic carbon in permafrost terrain using machine learning: A case study in a sub-arctic peatland environment. *Biogeosciences, 15*(6), 1663–1682. https://doi.org/10.5194/bg-15-1663-2018

Sorenson, P. T., Quideau, S. A., & Rivard, B. (2018). High resolution measurement of soil organic carbon and total nitrogen with laboratory imaging spectroscopy. *Geoderma, 315*, 170–177.

Soriano-Disla, J. M., Janik, L. J., ViscarraRossel, R. A., MacDonald, L. M., & McLaughlin, M. J. (2014). The performance of visible, near-, and mid-infrared reflectance spectroscopy for prediction of soil physical, chemical, and biological properties. *Applied Spectroscopy Reviews, 49*(2), 139–186.

Stenberg, B. (2010). Effects of soil sample pretreatments and standardised rewetting as interacted with sand classes on Vis-NIR predictions of clay and soil organic carbon. *Geoderma*. https://doi.org/10.1016/j.geoderma.2010.04.008

Sun, W., Zhu, H., & Guo, S. (2015). Soil organic carbon as a function of land use and topography on the Loess Plateau of China. *Ecological Engineering, 83*, 249–257. https://doi.org/10.1016/j.ecoleng.2015.06.030

Tahmasbian, I., Xu, Z., Boyd, S., Zhou, J., Esmaeilani, R., Che, R., & Hosseini, B. S. (2018). Laboratory-based hyperspectral image analysis for predicting soil carbon, nitrogen and their isotope compositions. *Geoderma, 330*, 254–263.

Troch, P., van Loon, E., & Hilberts, A. (2002). Analytical solutions to a hillslope-storage kinematic wave equation for subsurface flow. *Advances in Water Resources, 25*(6), 637–649. https://doi.org/10.1016/S0309-1708(02)00017-9

Tucker, G. E., & Bras, R. L. (1998). Hillslope processes, drainage density, and landscape morphology. *Water Resources Research, 34*(10), 2751–2764. https://doi.org/10.1029/98WR01474

U.S. Geological Survey (USGS). (2021). *Global 30 arc-second elevation (GTOPO30)*. U.S. Geological Survey. Retrieved from https://earthexplorer.usgs.gov/.

Viscarra-Rossel, R. A. (2007). Robust modelling of soil diffuse reflectance spectra by "bagging- partial least squares regression". *Journal of Near Infrared Spectroscopy, 15*, 37–47.

Wei, X., Bai, X., Wen, X., Liu, L., Xiong, J., & Yang, C. (2023). A large and overlooked Cd source in karst areas: The migration and origin of Cd during soil formation and erosion. *Science of the Total Environment, 895*, Article 165126. https://doi.org/10.1016/j.scitotenv.2023.165126

Wiesmeier, M., Hübner, R., Barthold, F., Spörlein, P., Geuß, U., Hangen, E., Reischl, A., Schilling, B., von Lützow, M., & Kögel-Knabner, I. (2013). Amount, distribution and driving factors of soil organic carbon and nitrogen in cropland and grassland soils of southeast Germany (Bavaria). *Agriculture, Ecosystems & Environment, 176*, 39–52. https://doi.org/10.1016/j.agee.2013.05.012

Wilson, J. P., & Gallant, J. C. (Eds.). (2000). *Terrain analysis: Principles and applications* (p. 479). New York, Chichester: Wiley.

Xue, R., Yang, Q., Miao, F., Wang, X., & Shen, Y. (2018). Slope aspect influences plant biomass, soil properties and microbial composition in alpine meadow on the Qinghai-Tibetan plateau. *Journal of Soil Science and Plant Nutrition*. https://doi.org/10.4067/S0718-95162018005000101 (ahead), 0.

Yang, M., Xu, D., Chen, S., Li, H., & Shi, Z. (2019). Evaluation of machine learning approaches toPredict soil organic matter and pH using vis-NIR spectra. *Sensors, 19*(263), 1–14.

Yimer, F., Ledin, S., & Abdelkadir, A. (2006). Soil organic carbon and total nitrogen stocks as affected by topographic aspect and vegetation in the Bale Mountains, Ethiopia. *Geoderma, 135*, 335–344. https://doi.org/10.1016/j.geoderma.2006.01.005

Zhang, P., Liu, L., Yang, L., Zhao, J., Li, Y., Qi, Y., & Cao, L. (2023). Exploring the response of ecosystem service value to land use changes under multiple scenarios coupling a mixed-cell cellular automata model and system dynamics model in Xi'an, China. *Ecological Indicators, 147*, Article 110009. https://doi.org/10.1016/j.ecolind.2023.110009

Zhang, G., Zhao, Z., Yin, X., & Zhu, Y. (2021). Impacts of biochars on bacterial community shifts and biodegradation of antibiotics in an agricultural soil during short-term incubation. *Science of the Total Environment, 771*, Article 144751. https://doi.org/10.1016/j.scitotenv.2020.144751

Zhang, G., Zhao, Z., & Zhu, Y. (2020). Changes in abiotic dissipation rates and bound fractions of antibiotics in biochar-amended soil. *Journal of Cleaner Production, 256*, Article 120314. https://doi.org/10.1016/j.jclepro.2020.120314

Zhou, G., & Yang, Z. (2023). Analysis for 3-D morphology structural changes for underwater topographical in Culebrita Island. *International Journal of Remote Sensing, 44*(7), 2458–2479. https://doi.org/10.1080/01431161.2023.2201386

Zhu, M., Feng, Q., Qin, Y., Cao, J., Li, H., & Zhao, Y. (2017). Soil organic carbon as functions of slope aspects and soil depths in a semiarid alpine region of Northwest China. *Catena, 152*, 94–102. https://doi.org/10.1016/j.catena.2017.01.011

Zhu, G., Liu, Y., Shi, P., Jia, W., Zhou, J., Liu, Y., & Zhao, K. (2022). Stable water isotope monitoring network of different water bodies in Shiyang River basin, a typical arid river in China. *Earth System Science Data, 14*(8), 3773–3789. https://doi.org/10.5194/essd-14-3773-2022

Zhu, H., Wu, J., Guo, S., Huang, D., Zhu, Q., Ge, T., & Lei, T. (2014). Land use and topographic position control soil organic C and N accumulation in eroded hilly watershed of the Loess Plateau. *Catena, 120*, 64–72. https://doi.org/10.1016/j.catena.2014.04.007